Report of the ASAC Subcommittee on Site and Stringency

Neal Evans, John Richer, Seiichi Sakamoto, Christine Wilson, Diego Mardones, Simon Radford, Selby Cull, Robert Lucas

1. Introduction

The ACC charged the ASAC to address the following issue:

The ASAC is asked to evaluate all available site (225 GHz opacity, 12 GHz phase stability, 350 micron and > 1 THz) data for Chajnantor, and to discuss any significant trends and issues which may impact the scientific mission, design or mission emphasis of the baseline instrument.

This issue was considered closely related to the considerations of stringency that have emerged from our thinking about operations and scheduling. Consequently, the ASAC asked that the definition of stringency be considered as part of this work.

The ASAC appointed a committee to address this issue, consisting of five ASAC members (Neal Evans, Chris Wilson, John Richer, Seiichi Sakamoto, and Diego Mardones), Simon Radford, Selby Cull (a summer student at NRAO-Tucson), and Robert Lucas. The ASAC members have supplied sample experiments that explore the parameter space of stringency. Radford and Cull have analyzed the site statistics. Lucas has considered the effect of these considerations on the ALMA simulator (delivering stringency estimates) and dynamic scheduler (incorporating stringency into the scheduler).

The committee decided to stick with the definition of stringency in the Fall 2002 ASAC report:

$$S = t_a/t_p,$$

where t_a is the total available time and t_p is the total time during which the conditions for the observations are met. After discussing the available site statistics, we decided to estimate S based on the NRAO site statistics on $\tau(225)$, ϕ_{rms}, and wind speed accumulated since 1995. While there are other data from Pampa La Bola, the time base is shorter, so we deferred incorporation of those data.

The wind data are used to ask whether the primary pointing specfications are met; that is, we restrict ourselves to a either/or decision. If the wind is less than 6 m s^{-1} in the daytime or 9 m s^{-1} in the nighttime, we assume the pointing specification of 0.6 arcseconds to be met. This simple assumption is satisfactory for now, but it should be reassessed once the actual performance is determined.

The yes/no wind criterion leaves two continuous variables. While there are diurnal, seasonal, and longer trends, we focus on the aggregate data over the period since 1995. Diurnal and seasonal trends are clearly present, as shown below; these may need to be considered in detailed planning. It is possible to compute S from the fraction of the time that both $\tau(225)$ and ϕ_{rms} are less than given values. We will show essentially the distribution function for $1/S$ in the last two figures. We also supply relations to relate the effective seeing angle ($\theta(see)$) to the phase noise. We also discuss improvements due to the water vapor radiometers and/or fast switching.

Next we present the example observations. The site statistics and stringency results are presented in the following section, followed by a discussion of the effects of phase correction. Then there is a discussion of the consequences for software and conclusions.

2. Examples of Observations

1. This will be a modest stringency experiment. Detect absorption by molecular line against the continuum of a disk. The model is the detection of formaldehyde at 1.3 mm in IRAS4A by Di Francesco et al. 2001, ApJ 562, 770. Using IRAM, they detected H_2CO absorption at 1.3 mm of $T_b = 10$ K against a continuum of 3000 mJy. They used a velocity resolution of 0.16 km/s. This provides the best evidence for infall, but it is currently only possible for the few brightest sources. To generalize the result and to study the infall velocity field in detail, we would like to do similar experiments on sources with 10 times weaker disks with velocity resolution of 0.05 km/s. Thus we need rms noise of 0.1 K for 10 sigma

detection. This could be done with modest spatial resolution, such as 1". Then we estimate the rms noise for 1 km/s resolution at 1.3 mm to be 0.29 K in 1 min. That indicates 168 min or 2.8 hours to achieve rms noise of 0.1 K with spectral resolution of 0.05 km/s and spatial resolution of 1". Since we are working at 1.3mm, the constraint on tau is very modest, say less than 0.1. Seeing constraint is also modest at say 0.5". Pointing just needs to meet spec. With the equations given below, the seeing constraint translates to a measured $\phi_{rms} = 3.2$ deg.

2. This will be about the highest stringency. We want to map a disk at the highest possible resolution. That means going to 0.35 mm in the largest array. Some probably out-of-date calculations indicate that we get a beam of 8.6 mas or 1.2 AU at 140 pc and can detect 71 earth masses of gas plus dust in 1 min. So we need the best tau and seeing, with great phase correction, and pointing in spec. Using the Matsushita conversion to 875GHz, we need $\tau(225) < 0.043$ to get $\tau(875GHz) < 1$. To get down to say 8 M_{earth}, we need these conditions for 1 hour. Let us say that we need $\theta(see) = 5$ mas. This translates to $\phi_{rms} = 0.12$ deg.

3. A deeply dust enshrouded super star cluster may only be detectable in the mm/submm continuum. To clearly identify such a cluster requires a spatial resolution of roughly 1 pc at a distance of 10-20 Mpc for typical cluster-containing galaxies. So we need angular resolution of 0.01-0.02″ and sufficient sensitivity to detect a dust signal that is equivalent to at least 10^6 and preferably 10^5 or 10^4 solar masses of gas. At 850 microns, this requires us to detect a source of 50-250 microJy at, say, the five sigma level in continuum. Primary stringency requirement: atmospheric stability to get 0.01-0.02″ resolution at 850 microns. This translates to $phirms = 0.26$ deg, and we take $\tau(225) = 0.1$ as our requirement.

3. Site Characteristics

On a high altitude (5050 m) plateau near Cerro Chajnantor in the Andes of northern Chile, the ALMA site is one of the best known locations for astronomy at millimeter and submillimeter wavelengths. Atmospheric conditions at Chajnantor have been studied extensively during the ALMA development phase and have been reviewed elsewhere (Radford & Holdaway 1998, Radford 2002). NRAO installed an instrument suite in 1995 April and ESO installed complementary instruments in 1998 June. On Pampa la Bola, about 8 km NE of the ALMA site, the Japanese installed monitoring instruments in 1996 June and the ASTE telescope in 2002 February. The NRAO and ESO instruments include a 225 GHz tipping radiometer, two 11.2 GHz interferometers, two 183 GHz line radiometers, a 350μm broadband tipping radiometer, and meteorology instruments. In addition, two groups have measured the atmospheric brightness at submillimeter wavelengths with Fourier Transform Spectrometers at Chajnantor (Matsushita et al. 1999, Paine et al. 2000).

At both 225 GHz and 350μm, the atmospheric transparency at Chajnantor is better more often than at Mauna Kea (Fig. 1). Only the South Pole enjoys comparable conditions (Radford & Chamberlin 2000, Radford 2002). At Chajnantor, the transparency shows significant seasonal and diurnal variations. Conditions are consistently good from April through December but deterioriate during January, February, and March (Fig. 2). In northern Chile, the summer months are known paradoxically as the "Bolivian winter" because a shift in the atmospheric circulation patterns draws moist air over the Andes from the Amazon basin. There is considerable year-to-year variation in the severity of this summer season. Even during the worst months on record, however, the median 225 GHz optical depth at Chajnantor, $\tau_{225} \approx 0.3$, is comparable to good conditions at many established observatories for millimeter wavelength astronomy. Diurnal transparency variations (Fig. 3) lag behind the solar cycle, with the best conditions occurring around sunrise. The diurnal variations are weaker during the winter than during the summer.

At Chajnantor, the atmospheric phase fluctuations on 300 m baselines are measured at 11.2 GHz by small interferometers observing beacons broadcast by communications satellites. For millimeter wavelengths, at least, these measured fluctuations can be scaled linearly with frequency to estimate the conditions at higher frequencies. For submillimeter wavelengths, however, dispersion at the edges of the windows becomes significant (Holdaway & Pardo 2001), so the measurements provide an underestimate of observing conditions. The phase stability is better in winter (Fig. 4), the diurnal phase stability variation (Fig. 5) is larger than the seasonal variation, the diurnal variation is more pronounced in phase stability than in transparency, and the diurnal phase stability variation more nearly matches the solar cycle than the diurnal transparency variation.

Two methods have been suggested to relate the measured fluctuations to image quality (Table 1). Holdaway and Owen (1995) estimated the highest frequency where the phase fluctuations on 300 m baselines would allow good imaging (30° r.m.s.) or any image reconstruction at all (70° r.m.s.). Masson (1994) extrapolated the temporal structure function of the observed fluctuations to estimate the baseline, $b_{\max}$, where the phase fluctuations at 345 GHz are 1 radian r.m.s. and the corresponding angular resolution limit, or seeing, $\theta(see) = 0.7\lambda/b_{\max} = 0.14'' \ \lambda(mm)/b_{\max}(km)$. Essentially, one is simply limited in resolution by the largest usable baseline. To calculate the largest usable baseline, we first need to scale the measured ϕ_{rms} in degrees to the observed airmass (A), frequency (ν) and baseline (b) from

ϕ_{rms} at the site testing parameters (A = 1.7, ν = 11.2 GHz, and b = 0.3 km). For this report, we use the following: $\phi_{rms}(A,\nu,b) = \phi_{rms}(1.7, 11.2, 0.3)(A/1.7)^{0.5}(\nu/11.2)(b/0.3km)^s$ where the phase noise is assumed to increase as the square root of the air mass, linearly with frequency, and with baseline as the power s. We then set the phase fluctuations to the largest allowable phase fluctuations (in the example given here, 1 rad) and solve for b_{max}: $b_{max} = 0.3\mathrm{km}[(11.2GHz/\nu)(1.7/A)^{0.5}(57.3/\phi_{rms}(A,\nu,b)]^{1/s}$. Finally, $\theta(see) = 0.47''\lambda(mm)[(\nu/11.2GHz)(A/1.7)^{0.5}(\phi_{rms}/57.3)]^{1/s}$, where ϕ_{rms} is the value from the site testing interferometer (note however that in some plots, it is already corrected to $A = 1$). The value of s changes with baseline, but we will approximate it here by $s = 0.6$. This is the median exponent on the structure functions of the measured data (Holdaway and Pardo 2001). In Table 1 below, we apply these equations to the case of observing at 345 GHz (λ = 0.87 mm) at the zenith ($A = 1$); note that the ϕ_{rms} values in the table are already referred to the zenith!. The equation becomes $\theta(see) = 0.093''(\phi_{rms})^{1.67}$ One can easily substitute for other observing parameters or assumptions about the structure function.

Most of the time at Chajnantor, phase stable observations are possible only for long wavelengths or short baselines. To achieve the ALMA performance goals, compensation for atmospheric phase fluctuations will be necessary much of the time for millimeter wavelengths and modest baselines and most of the time for submillimeter wavelengths and long baselines.

Because of differences in instrument configuration and other factors, it is more complicated to compare phase fluctuation measurements at different sites than transparency measurements. Nonetheless, a quick estimate based on Masson's method (1994) indicates the median limiting angular resolution at Chajnantor is about twice as good as at Mauna Kea.

Table 1: Chajnantor phase stablility

measured ϕ_{rms}			ν_{limit} [GHz]		345 GHz	
	[μm]		30°	70°	b_{max} [m]	θ_{see}
75 %	394	5.3°	63	148	52	2.40″
50 %	187	2.5°	134	313	181	0.69″
25 %	89	1.2°	281	655	625	0.20″
10 %	49	0.7°	510	1189	1691	0.07″

ϕ_{rms}: r. m. s. fluctuations on a 300 m baseline at 11.198 GHz at 36° elevation over 10 min intervals **referenced to the zenith**. ν_{limit}: frequency limit for observations with specified r. m. s. phase fluctuations (Holdaway & Owen 1995). b_{max} [m] and θ_{see}: maximum usable baseline and effective seeing at 345 GHz (Masson 1994) calculated for the median structure function exponent, 0.6 (Holdaway and Pardo 2001).

Several atmospheric parameters show significant correlation, but others are only weakly correlated at best. To illustrate these correlations in the presence of substantial scatter, the data were selected on the value of one parameter and then distributions of a second parameter were compiled. The comparisons show westerly winds are stronger than easterly winds (Fig. 6), the transparency is better during colder periods (Fig. 7) and during westerly winds [currently this plot shows wind speed, not direction. NJE] (Fig. 8), and the phase stability is better during weaker winds (Fig. 9). and colder periods (Fig. 10). Despite a tremendous scatter, there is a significant correlation between the transparency and the phase stability. When the transparency is better than the median, the phase stability is about twice as good as otherwise (Fig. 11).

The atmospheric data are recorded every 10 min. To evaluate conditions over longer intervals, cumulative distributions were compiled for the median or the maximum during the interval. As expected, there is essentially no change in the distributions of the medians (Fig. 12). For the maxima, on the other hand, the distributions show a monotonic degradation with interval length (Fig. 13). This is more pronounced for the phase fluctuations than for the transparency (Fig. 14).

In Figure 15, we have plotted the two-dimensional probability density $P(\phi,\tau)$. The contours encircle 5, 10, 15, ... per cent of the total probability. Although typical conditions are of course excellent, there is a significant amount of time with less good conditions. Note especially the relatively long tail on the phase stability distribution. The correlation of τ and ϕ has substantial scatter. We have also shown the joint probability densities (Fig. 16) of the opacity and phase stability when the wind speed is such that the pointing specifications will be met (speed is $>$ 6 m/s at day, or $>$ 9 m/s at night time). Note that the wind conditions are met only 55% of the time, so the outermost contour is the 50% contour. Note the substantial growth in the contours, especially outside the 25% contour, when the wind condition is applied.

4. Phase correction schemes

The Chajnantor site has, for a ground-based site, excellent transparency and good phase stability. Nonetheless, the accurate atmospheric phase correction is a critical requirement for practically all ALMA observations. ALMA will use a combination of fast-switching and 183GHz radiometric measurements to correct for atmospheric phase fluctuations: the phase correction problem is so critical to achieving ALMA's science goals that this apparent redundancy in the project plan is vitally important. Although the solutions in the project plan should achieve accurate phase measurements, correcting atmospheric phase on 10 km baselines at 650 GHz is non-trivial, and is a unique problem for ALMA. How these two techniques will be used together is still unclear, and it likely that this will evolve with experience. The importance of continuing efforts into phase correction techniques cannot be stressed enough if ALMA is to succeed.

4.1. Fast switching

There are many very detailed memos, many written by Mark Holdaway, which put together the expected source counts and measured atmospheric fluctuations to estimate the effectiveness of fast switching as a phase correction technique. These are non-trivial simulations to perform, being technically complex and requiring detailed simulation of the observing and data reduction process. Memo 403 nicely brings these results up to date for an ALMA design of 64 12-m antennas. The bottom line is that fast switching, with a few caveats, should work well for ALMA at all frequencies, achieving phase errors less than 25 degrees rms at all frequencies on all baselines. 25 degrees is taken as the phase rms goal as it allows good imaging quality. The total efficiency of fast switching, including losses due to decorrelation and time spent on the phase calibrator, is principally a function of phase fluctuations and airmass, but is typically better than 90% in these simulations. This calculation assumes that one schedules observing programmes based on the current phase stability — i.e one matches high frequency programmes to the periods of highest phase stability. Although this assumption is sensible for first-order models, the plot above showing the poor correlation of τ and ϕ_{rms} means that a more sophisticated set of simulations would be useful. In particular, we will most likely have to consider both τ and ϕ_{rms}. And it is clear that in periods of good opacity, there is a significant amount of poor seeing.

For example, considering only the best weather ($\tau < 0.05$), the rms phase fluctuations at 11 GHz are 0.95 (25th centile), 1.7 (median), 3.6 (75th centile) and 7.0 (90th centile) degrees. For weather better than $\tau < 0.036$, the corresponding numbers are 0.8, 1.5, 3.0 and 5.8 degrees. For reference, the 10th centile of the entire phase statistics is only 0.83 degrees. In summary, about a quarter of the lowest opacity weather has a phase stability worse than 3 degrees at 11GHz. Bearing in mind that we are likely to be observing at high frequencies in such good weather, these are significant fluctuations: for example, ignoring the dispersive effect, this scales up to 180 degrees of phase at 650 GHz on 300-m baselines. It is unlikely that fast switching will be effective in these conditions, although more simulations are needed to demonstrate this.

4.2. Radiometric phase correction

There is much less concrete data from which we can make predictions about the effectiveness of radiometric phase correction techniques. We are heavily reliant at the moment on theoretical models and sensitivity estimates, plus a very small number of results from the JCMT-CSO, and the test systems on Chajnantor. Modeling radiometric phase corrections is even more complex than modeling fast switching, involving as it does detailed atmospheric models, and we have very little quantitative to go on at the present time. Fast switching is the standard technique at cm wavelengths, and the theoretical models seem to be well supported by experimental data. There are few such constraints using the 183 GHz line, as observational results are so scarce. It remains of high importance to the ALMA project that a coherent programme of work on both simulations and real tests is carried out over the coming years.

The project specifications for WVR corrections are established in memos 303 and 352. The aim is to correct the path to each antenna to an accuracy of $10(1 + w_v)\,\mu$m, where w_v is the line-of-sight water vapour content in mm. This correction must be made in one second of time, and be reliable over a 5 minute period, with modest changes in zenith angle or airmass allowed (at the moment the specification is a zenith angle change of less than one degree). At 900 GHz, with $w_v = 1$ this corresponds to a phase error of 22 degrees.

In principle, these specifications, if met by the WVR system, would allow us to phase correct essentially all data to an accuracy of 25 degrees of better, allowing diffraction-limited imaging at all frequencies with high efficiency on all baselines. But this remains a significant challenge to both the WVR hardware and our atmospheric models.

It is important to recall that the possibility of correcting the phase gradient across the 12-m aperture (which effectively adds a pointing error) was not adopted by the project, although should be possible with extra effort and resources.

The advantages of using the radiometric technique in conjunction with fast-switching, rather than fast-switching alone, include

- an increase the integration time on source, both reducing decorrelation losses and reducing wear-and-tear on the antenna drives
- an increase in the correlation amplitude accuracy
- the potential to achieve even higher phase stability, so improving image quality
- the potential to allow efficient use of the very low τ weather when phase stability is poor.

In extreme cases, it may well prove that using the radiometers allow useful observations in very unstable periods when fast switching is ineffective, but this is as yet mere speculation. Unfortunately, all these statements are qualitative. A good deal of further simulation will be needed, and experimental data obtained, before they can be quantified.

5. Software implications

Requirements have been discussed by the SSR, and are available at

`http://iraux2.iram.fr/%7Elucas/almassr/report-2/report-2-v4r2.pdf` [1]

The sections relevant here are Dynamic Scheduling (3.4) and Simulation (3.8).

5.1. Dynamic Scheduling

Programmes will be split into scheduling blocks; the scheduling block priorities will be reevaluated at the end of execution of each block (long programmes will be obtained by repeated execution of the same block). The priorities will include many factors, some trivial (e.g. source visibility), other highly fluctuating like phase rms and system temperature (atmosphere included). Both science rating and stringency will be primary factors.

The SSR required that the dynamic scheduler should be its own simulator, as it can be executed with atmospheric data (as we already have) and a set of scheduling blocks as input, to tune up the formula and coefficients for optimum use of ALMA during a scheduling season:

"The actual formula and coefficients must be tuned for optimum overall efficiency, and agreement with observatory policy, according to the distribution of programme requirements and the weather statistics on the ALMA site. The ordering of programmes according to scheduling probabilities should match that of science ratings, in each range of observing conditions."

The conclusions of the present report call for treating the system temperatures (or opacities) and the phase rms as truly independent parameters, which had been foreseen. They should both appear as strict upper limits (a SB requiring e.g. less than 1mm precipitable H_2O and 50μm pathlength rms is not scheduled if either requirement is not met) and through the stringency factor (to make sure this SB is given priority over less demanding ones whenever these conditions are met).

5.2. Simulation

Memo 11 formulates requirements on ALMA simulator. The simulator should in principle allow to investigate the use of both fast switching and radiometric phase correction methods, by generating fake data using state-of-the-art atmosphere models, and processing them through the off-line data reduction package.

6. Summary

The data presented above lead us to the following conclusions.

[1] this link points to a new version of ALMA Software memo 11 that should still be regarded as a draft, until it is formally reviewed at the end of 2002 September; however this text takes into account the revieres' comments.

- With the either-or criterion on wind, there are large periods (about 45% of the time) when the pointing specification will not be met. It will be important to characterize with real antennas how the pointing actually degrades and to consider the consequences for effective utilization of ALMA.
- The values of $\tau(225)$ and $\phi(rms)$ are correlated, but there is a lot of scatter. In particular, there is a tail in Fig. 15 of relatively high $\phi(rms)$ at low $\tau(225)$.
- For high frequencies and/or long baselines, the phase fluctuations will limit resolution/fidelity. Achieving the full potential of ALMA will definitely require that the phase correction methods are effective.

If we apply the calculations to the examples given in §2, we find that experiment number 1 can be done about 30% of the time; if the pointing degrades gracefully, this percentage could be increased. Neither of the other examples could be done without phase correction in any significant fraction of the time. Assuming that phase correction works to the levels needed, experiment number 2 could be done about 17% of the time and and experiment number 3 could be done 39% of the time (these estimates include only the constraint on τ and assume that the pointing will be acceptable 55% of the time). These examples reinforce the conclusions drawn above.

6.1. References

Correcting for Decorrelation Due to Atmospheric Phase Errors,
Holdaway, M. A.& Owen, F. N., 1995, Millimeter Array Memo 136 (NRAO)

Atmospheric Dispersion and Fast Switching Phase Calibration,
Holdaway, M. A.& Pardo, J. R., 2001, Atacama Large Millimeter Array Memo 404 (NRAO)

Atmospheric Effects and Calibrations,
Masson, C. R., 1994, in Astronomy with Millimeter and Submillimeter Wave Interferometry, IAU Colloquium 140, ASP Conference Series, Vol. 59, M. Ishiguro and J. Welch, Eds., p.87

FTS Measurements of Submillimeter-Wave Atmospheric Opacity at Pampa la Bola II: Supra-Terahertz Windows and Model Fitting,
Matsushita, S., Matsuo, H., Pardo, J. R., & Radford, S. J. E., 1999, PASJ 51, 603

A Fourier Transform Spectrometer for Measurement of Atmospheric Transmission at Submillimeter Wavelengths,
Paine, S., Blundell, R., Papa, D. C., Barrett, J. W., & Radford, S. J. E., 2000, PASP 112, 108

Atmospheric Conditions at a Site for Submillimeter Wavelength Astronomy, Radford, S. J. E., & Holdaway, M. A., 1998, in Advanced Technology MMW, Radio, and Terahertz Telescopes, ed. Phillips, T. G., Proc. SPIE 3357, 486

Atmopsheric Transparency at 225 GHz over Chajnantor, Mauna Kea, and the South Pole,
Radford, S. J. E., & Chamberlin, R. A., 2000, Atacama Large Millimeter Array Memo 334.1 (NRAO)

Site Characterization for mm/submm Astronomy,
Radford, S., 2002, in Astronomical Site Evaluation in the Visible and Radio Range, ASP Conf. Ser. 266, ed. Vernin, J., Benkhaldoun, Z., & Muñoz-Tuñón, C. (San Francisco: ASP) p. 148

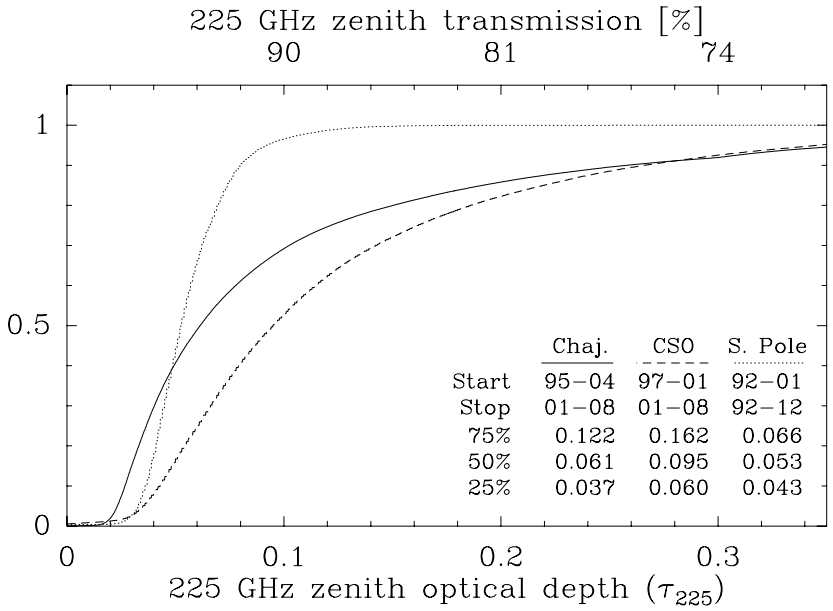

Fig. 1.— Cumulative distributions of the 225 GHz zenith optical depths (τ_{225}) measured at Chajnantor, at Mauna Kea (CSO), and at the South Pole. Adapted from Radford & Chamberlin (2000). The distributions of the broadband 350μm measurements are similar.

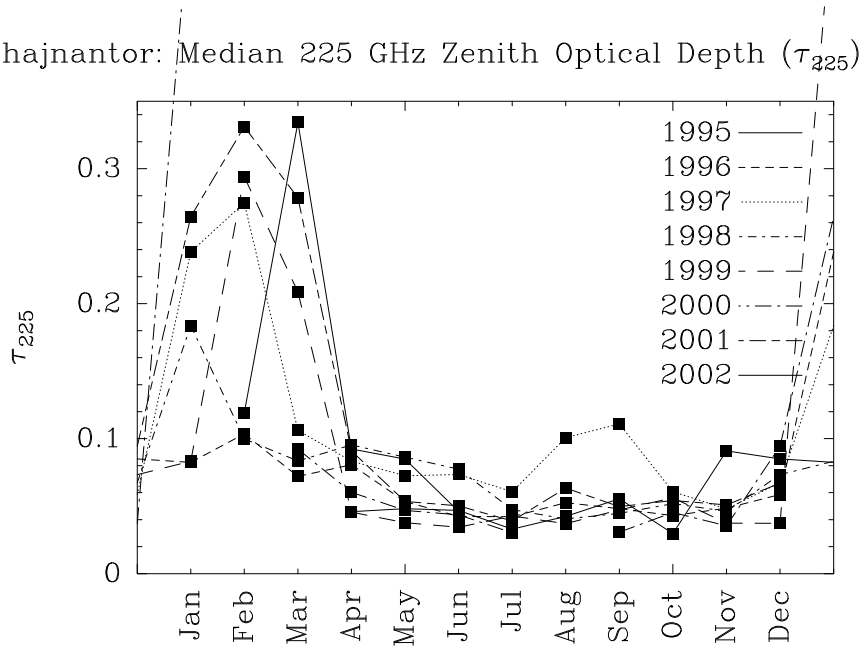

Fig. 2.— Seasonal variation of median measured 225 GHz zenith optical depths at Chajnantor. The variation of the broadband 350μm measurements is similar.

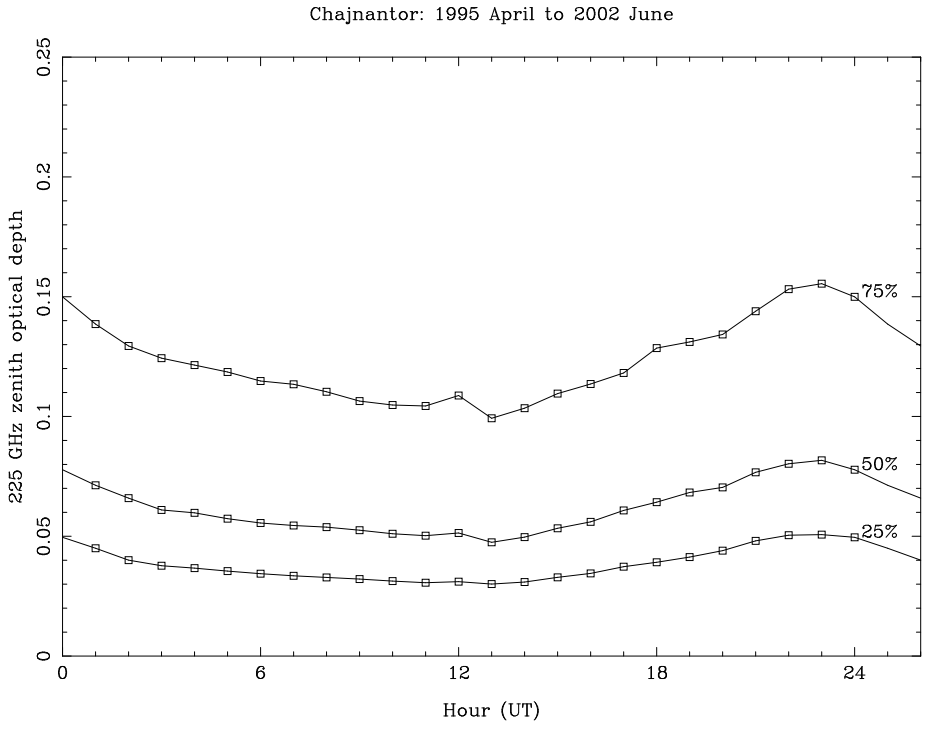

Fig. 3.— Diurnal variation of quartiles of measured 225 GHz zenith optical depths at Chajnantor. Local solar time is UT $- 4^{\rm h}\,31^{\rm m}$. The variation of the broadband 350μm measurements is similar.

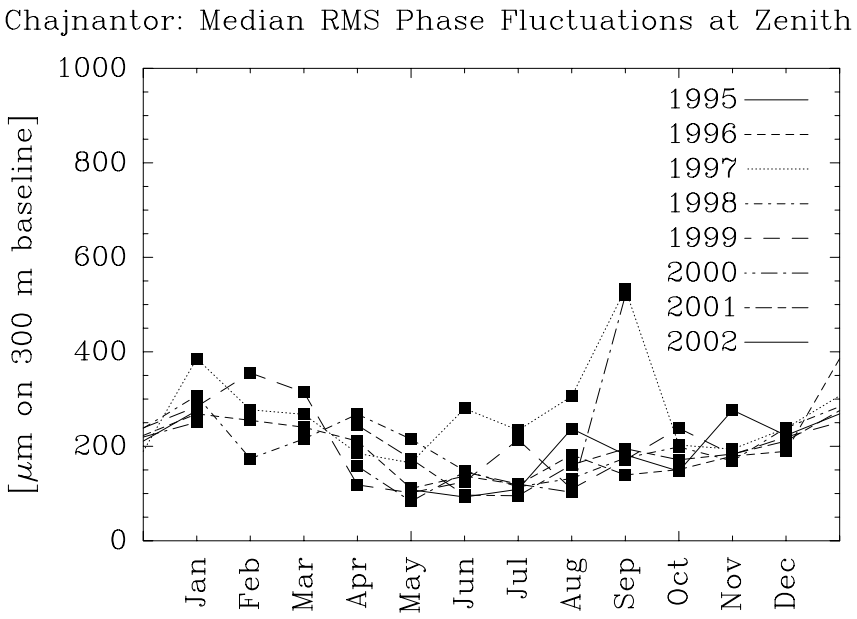

Fig. 4.— Seasonal variation of median measured phase fluctuations at Chajnantor referred to the zenith.

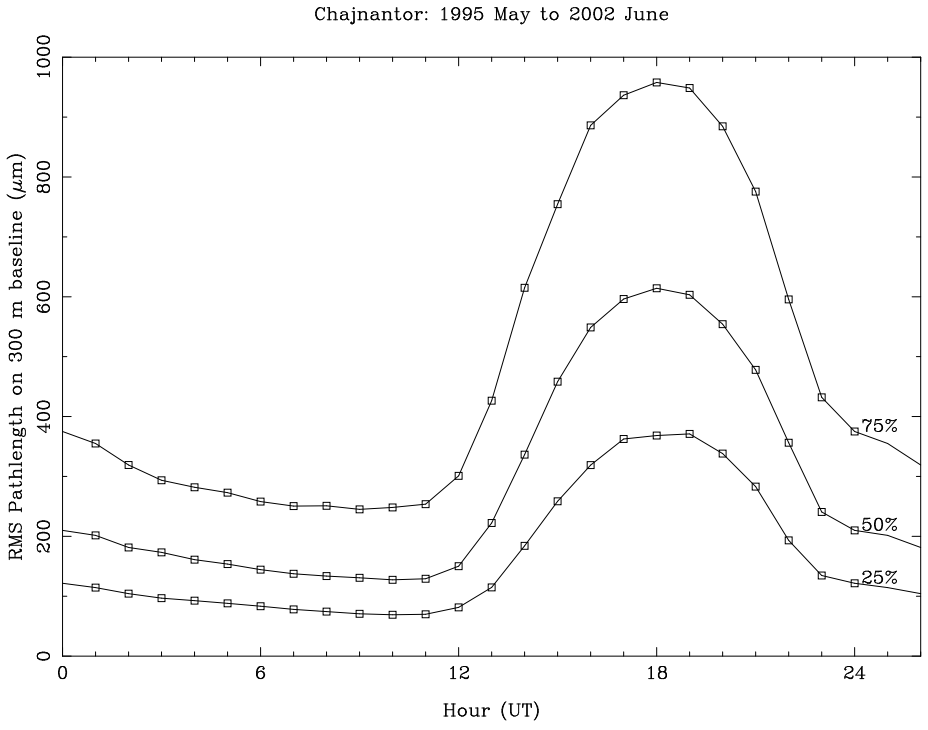

Fig. 5.— Diurnal variation of quartiles of measured phase fluctuations at Chajnantor referred to the zenith.

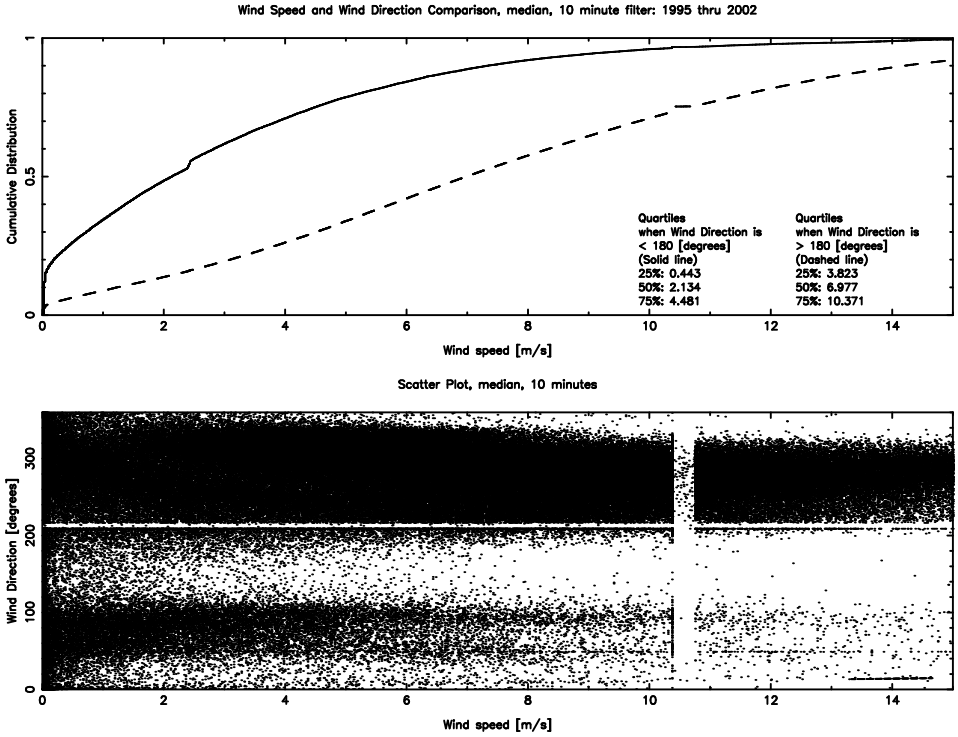

Fig. 6.— Cumulative distributions of westerly and easterly wind speeds measured at Chajnantor.

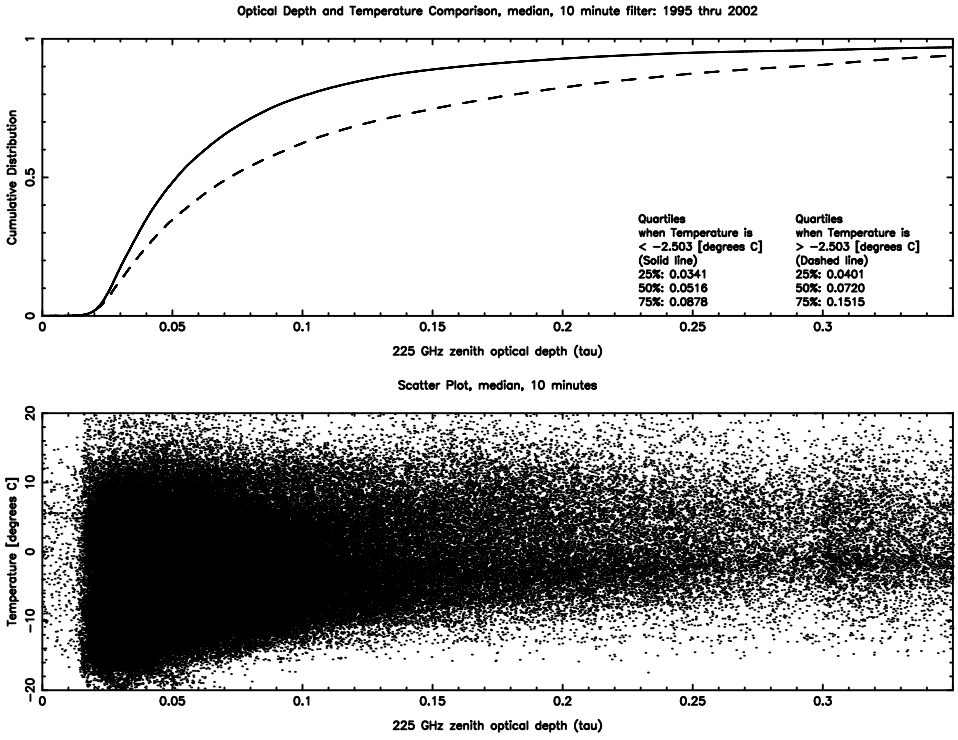

Fig. 7.— Cumulative distributions of the 225 GHz zenith optical depths (τ_{225}) measured at Chajnantor when the temperature was above or below the median.

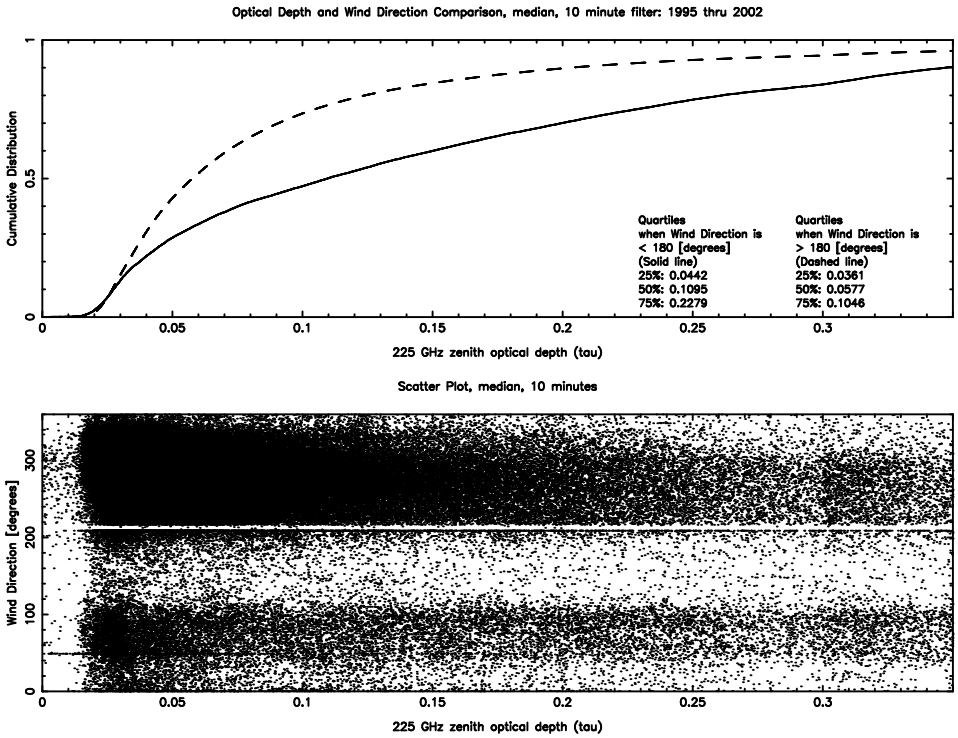

Fig. 8.— Cumulative distributions of the 225 GHz zenith optical depths (τ_{225}) measured at Chajnantor during westerly and easterly winds.

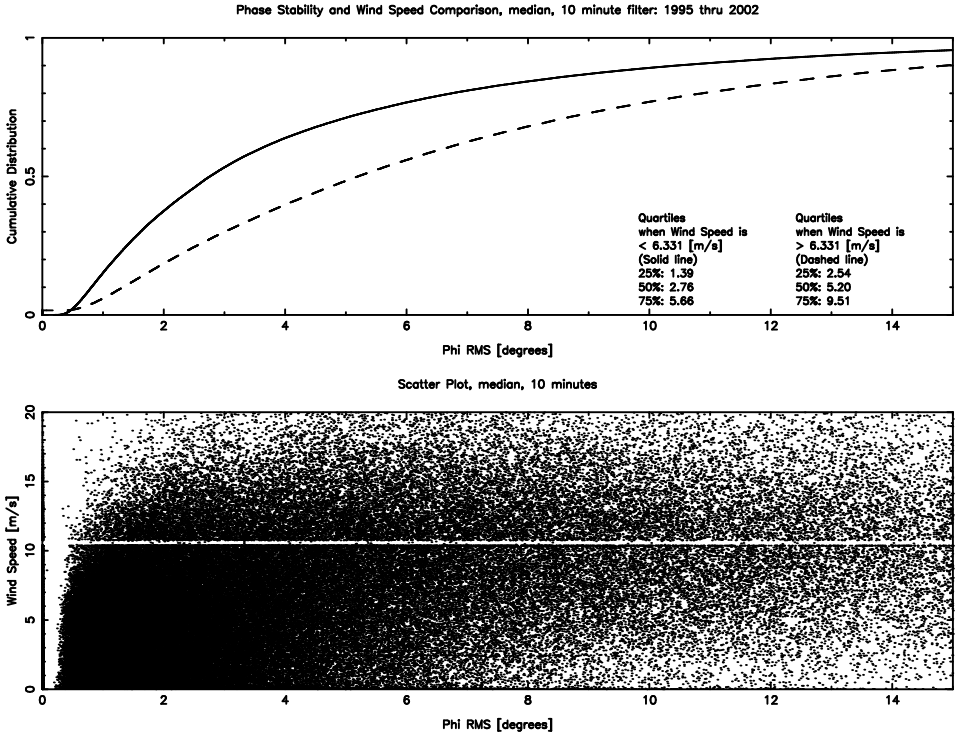

Fig. 9.— Cumulative distributions of the maximum 11.2 GHz phase fluctuations measured at Chajnantor when the wind speed was above or below the median.

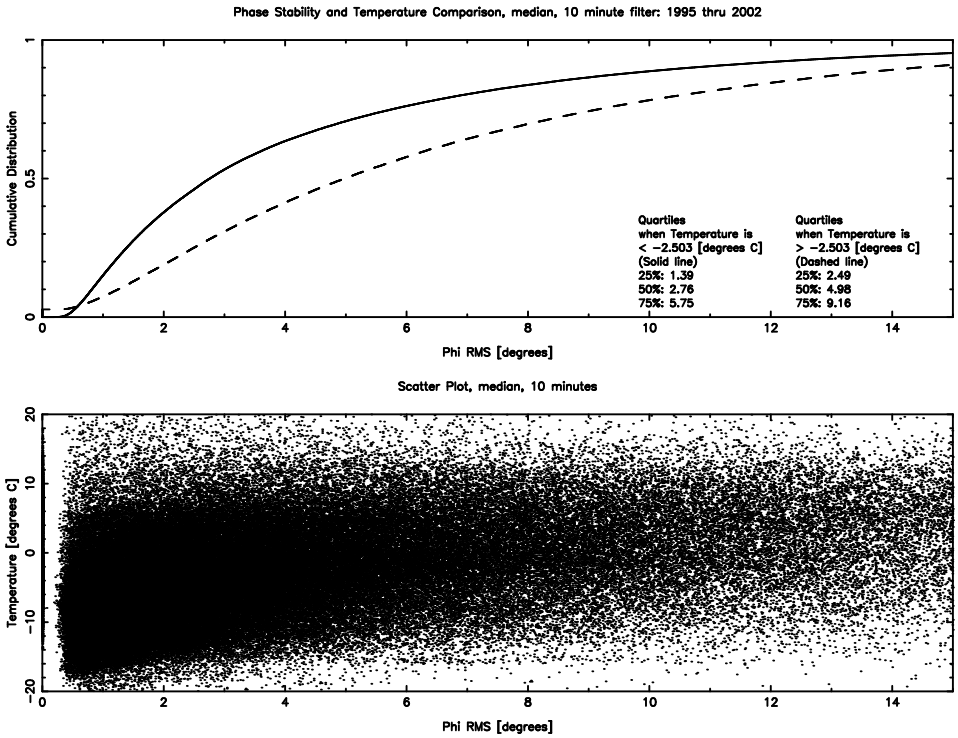

Fig. 10.— Cumulative distributions of the maximum 11.2 GHz phase fluctuations measured at Chajnantor when the temperature was above or below the median.

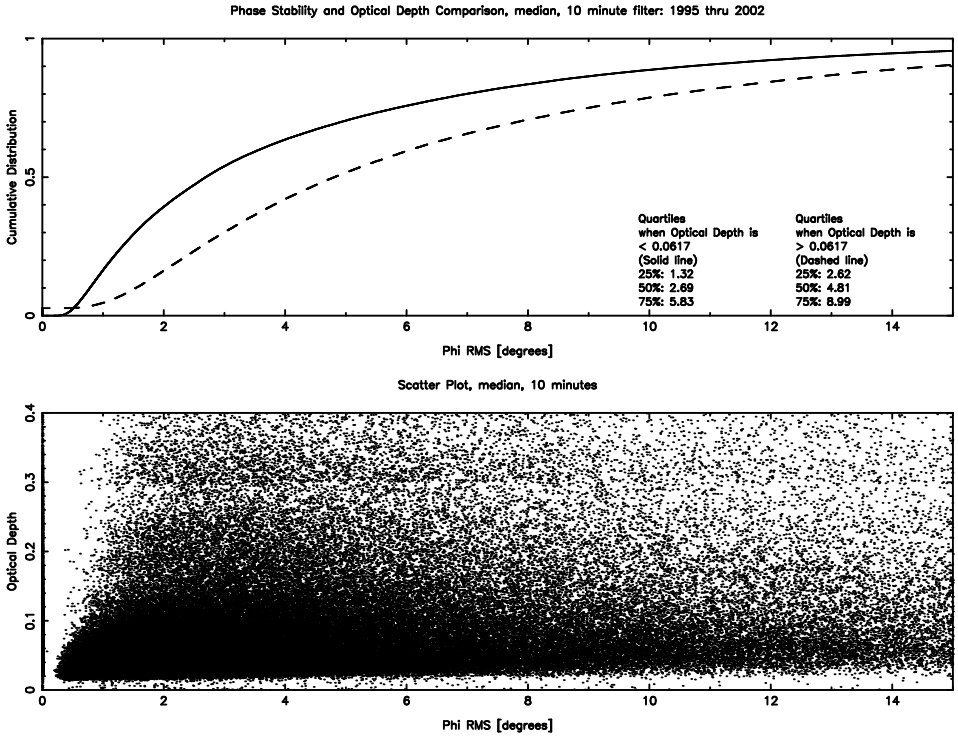

Fig. 11.— Cumulative distributions of the maximum 11.2 GHz phase fluctuations measured at Chajnantor when the 225 GHz zenith optical depth (τ_{225}) was above or below the median.

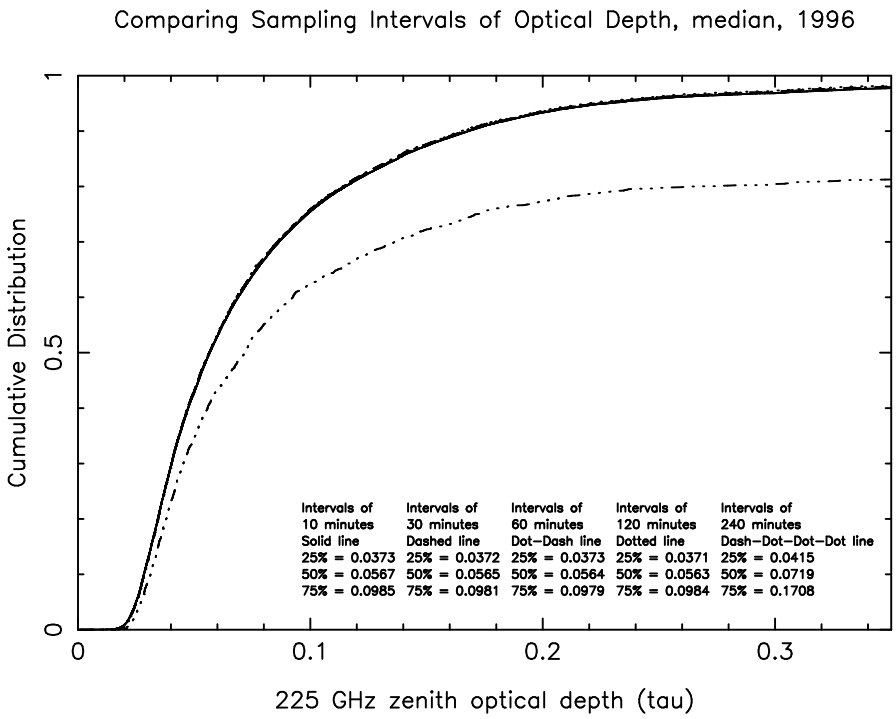

Fig. 12.— Cumulative distributions of the median 225 GHz zenith optical depths (τ_{225}) measured at Chajnantor in 1996 for different sampling intervals. The 240 min interval suffers from a processing defect.

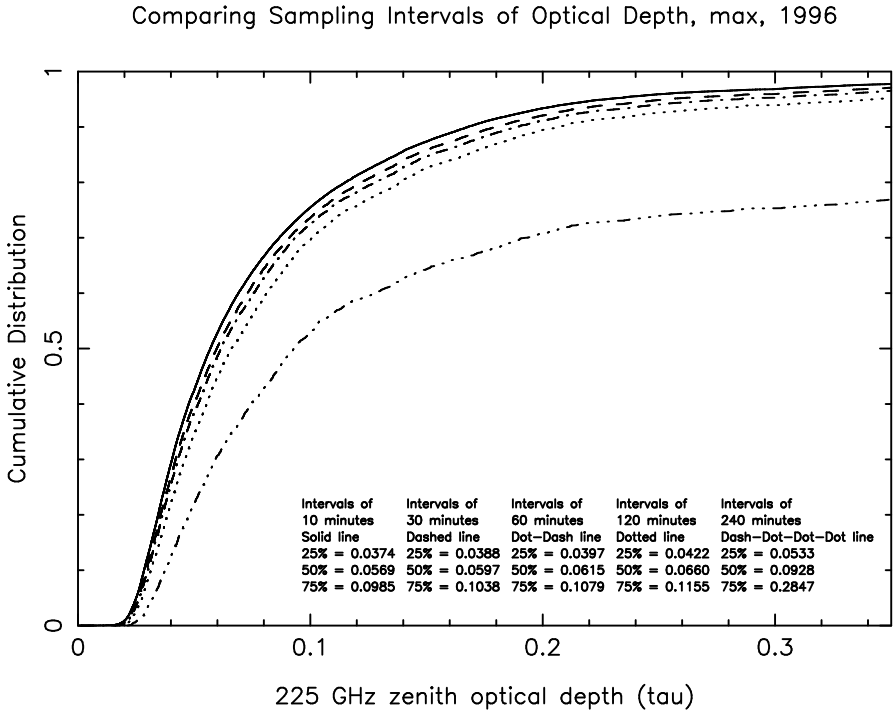

Fig. 13.— Cumulative distributions of the maximum 225 GHz zenith optical depths (τ_{225}) measured at Chajnantor in 1996 for different sampling intervals. The 240 min interval suffers from a processing defect.

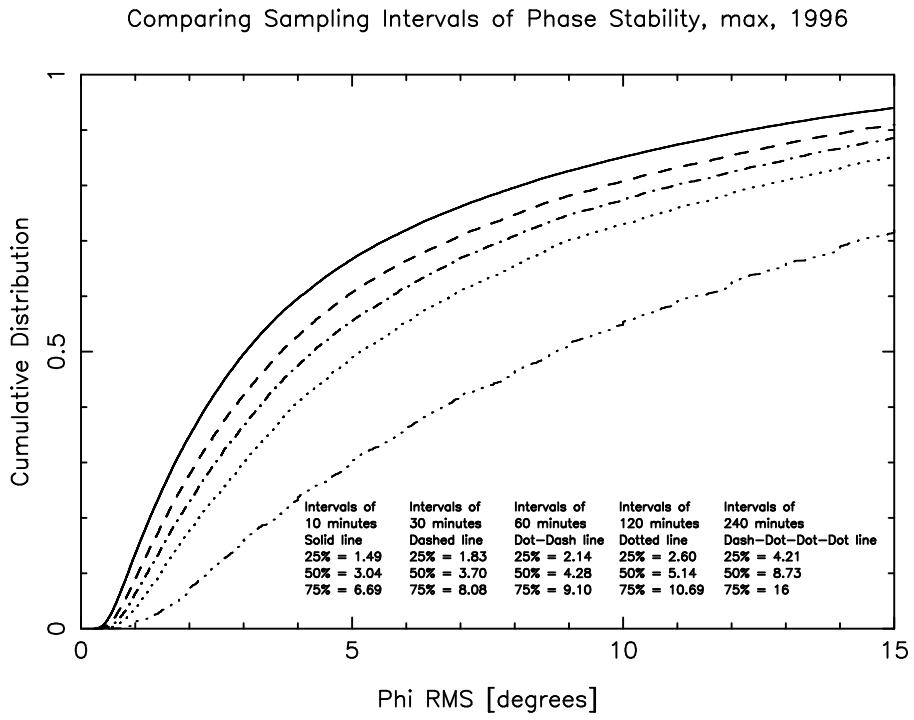

Fig. 14.— Cumulative distributions of the maximum 11.2 GHz phase fluctuations measured at Chajnantor in 1996 for different sampling intervals. The 240 min interval suffers from a processing defect.

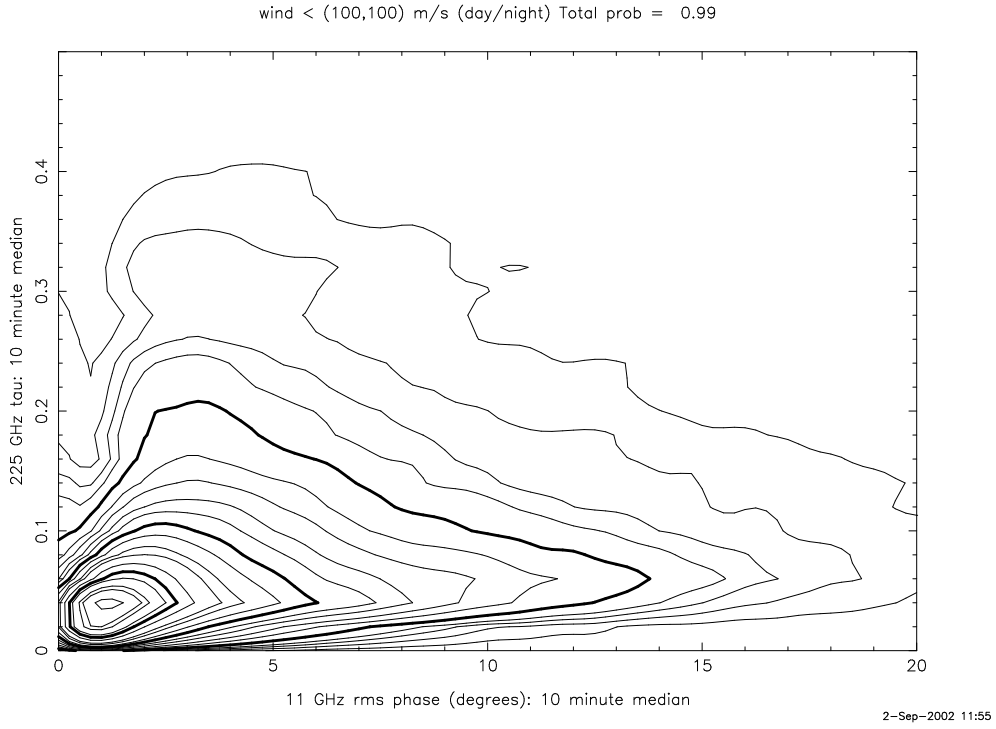

Fig. 15.— Joint probability distribution of $\tau(225)$ and $\phi(rms)$ with a very loose wind (pointing) requirement: that the wind speed be less than 100 m/s either day or night. The contours encircle 5, 10, 15, ... per cent of the total probability (99% in this case).

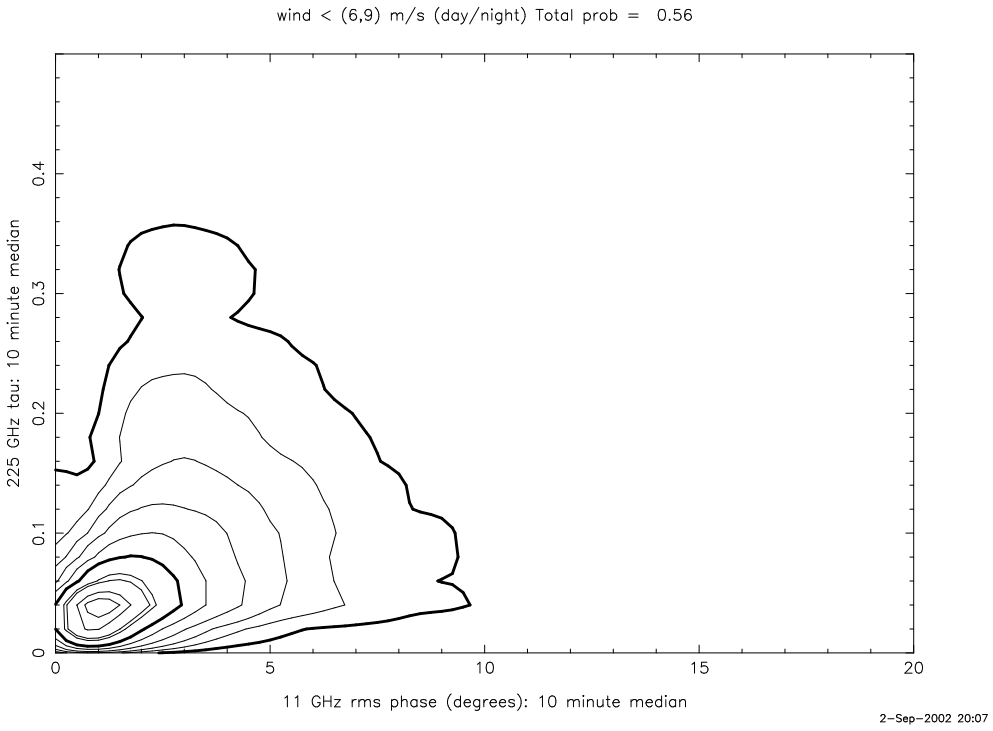

Fig. 16.— Joint probability distribution of $\tau(225)$ and $\phi(rms)$ with a the wind requirement that allows the pointing specification to be met: that the wind speed be less than 6 m/s in the daytime and less than 9 m/s at night. The contours encircle 5, 10, 15, ... per cent of the total probability (55% in this case).